ACS ORGANIC & INORGANIC Au
AN OPEN ACCESS JOURNAL OF THE AMERICAN CHEMICAL SOCIETY



pubs.acs.org/orginorgau
Article

# Hydrogen Oxidation by Bioinspired Models of [FeFe]-Hydrogenase

*Published as part of ACS Organic & Inorganic Au special issue "Electrochemical Explorations in Organic and Inorganic Chemistry".*

Abhijit Nayek, Rabin Kumar Poria, Md Estak Ahmed, Suman Patra, Somdatta Ghosh Dey,* and Abhishek Dey*

Cite This: *ACS Org. Inorg. Au* 2025, 5, 105−116
Read Online

ACCESS | Metrics & More | Article Recommendations | Supporting Information

**ABSTRACT:** Synthetic azadithiolate-bridged diiron clusters serve as structural analogues of the active site of [FeFe]-hydrogenases. Recently, an *o*-alkyl substitution of aniline-based azadithiolate bridge allowed these synthetic models to both oxidize $H_2$ and reduce $H^+$, i.e., bidirectional catalysis. Hydrogen oxidation by synthetic analogues of hydrogenases is rare, and even rarer is the ability of diiron hexacarbonyls to oxidize $H_2$. A series of synthetic azadithiolate-bridged biomimetic diiron hexacarbonyl complexes are synthesized where the substitution in the *para* position of the *ortho*-methyl aniline in the azadithiolate bridge is systematically varied between electron-withdrawing and electron-donating groups to understand factors that control $H_2$ oxidation by diiron hexacarbonyl analogues of [FeFe]-hydrogenases. The results show that the substituents in the *para* position of the *ortho*-ethyl aniline affect the electronic structure of the azadithiolate bridge as well as that of the diiron cluster. The electron-withdrawing $-NO_2$ substituent results in faster $H_2$ oxidation relative to that of a $-OCH_3$ substituent.

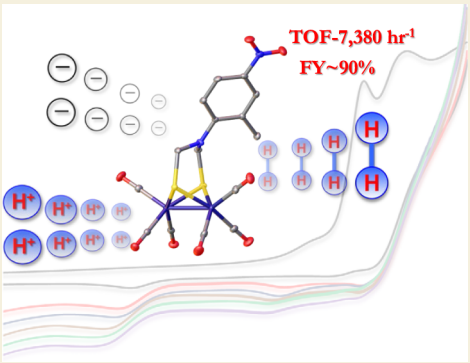


**KEYWORDS:** *hydrogen oxidation, hydrogenase, homogeneous electrocatalysis, model complex synthesis, structural tuning*

## INTRODUCTION

Hydrogen, obtained from sustainable sources, appears to be a cleaner alternative to fossil fuels.[1,2] Fuel cells oxidize hydrogen at the anode and reduce oxygen at the cathode, forming water and thereby converting the chemical energy stored in the H−H and O−O bonds into electrical energy. Chemical fuels such as hydrogen are ideal because of their high energy density by weight and pollution-free by products. The key to the success and large-scale deployment of fuel cells[3−5] is the availability of earth-abundant metal-based[6] cheap and efficient catalysts for the two half-cells involved (eqs 1 and 22). Presently, platinum stands as the most effective catalyst for hydrogen oxidation. However, its widespread application is restricted by its high cost and limited availability.[7,8] The designing of molecular catalysts by using earth-abundant metals for electrochemical hydrogen oxidation holds the potential to offer viable replacements for the costly platinum catalysts commonly employed in hydrogen fuel cells.[9] For hydrogen production, many molecular catalysts have been developed by using nontoxic, inexpensive, abundant metals such as nickel,[10−16] cobalt,[17−22] and iron.[23−27] There is a scarcity of reported homogeneous electrocatalysts for the oxidation of hydrogen for using efficiently in hydrogen fuel cells.[28−39]

$$\frac{1}{2}H_2 \rightleftharpoons H^+ + e^- \quad (E = -0.059V \cdot pH) \tag{1}$$

$$\frac{1}{2}O_2 + 2H^+ + 2e^- \rightleftharpoons H_2O \quad (E = 1.23V - 0.059V \cdot pH) \tag{2}$$

In nature, there are several organisms where hydrogen plays an important role in their metabolism and energy storage.[40,41] This vital process is orchestrated by metalloenzymes known as hydrogenases.[41−44] Among these, the [FeFe]-hydrogenase stands out for its remarkable ability to catalyze the oxidation of $H_2$ at rates as high as 28,000 $s^{-1}$, heralding the potential of bioinspired mimics of [FeFe]-hydrogenases as viable alternatives to precious metals in fuel cell applications.[45] The active site of [FeFe]-hydrogenase (Figure 1A) contains a [4Fe-4S] cluster and a [2Fe] subcluster. The [4Fe-4S] cluster is covalently linked via a cysteine residue to the binuclear [2Fe] subcluster.[46,47] Through X-ray crystallography[48,49] and spectroscopic analysis,[50,51] it has been confirmed that each of the two iron centers contains a terminal $-CN^-$ and a terminal $-CO$ ligand, with a $-CO$ ligand bridging both iron

Received: September 21, 2024
Revised: November 6, 2024
Accepted: November 20, 2024
Published: December 3, 2024

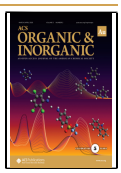





https://doi.org/10.1021/acsorginorgau.4c00073
*ACS Org. Inorg. Au* 2025, 5, 105−116

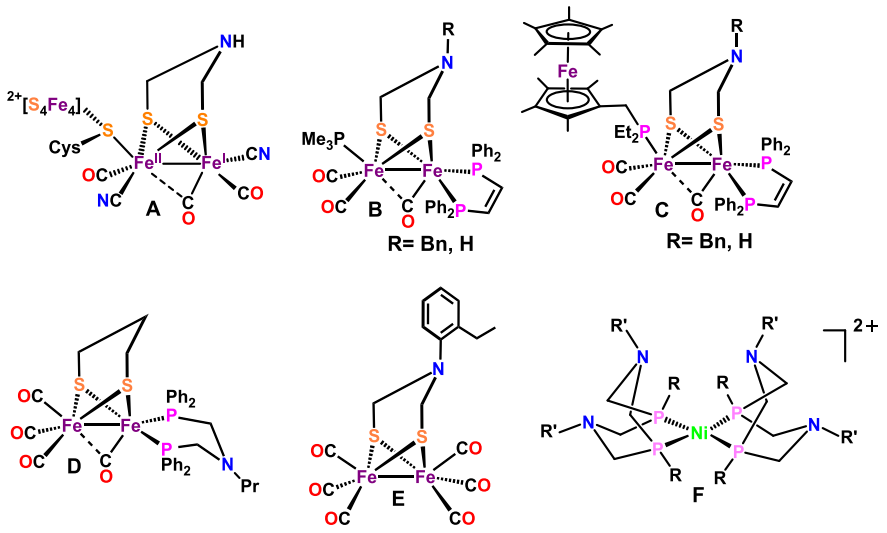


**Figure 1.** (A) Structure of the active site of [FeFe]-$H_2$ase (H-cluster, $H_{ox}$). (B–E) Previously reported [2Fe]-mimics that can activate $H_2$. (F) $[Ni(P^R_2N^{R'}_2)_2]^{2+}$ molecular catalyst.

centers.[52−54] The two diiron cores are bridged by an azadithiolate (ADT) ligand (−$SCH_2NHCH_2S$−).[53,55−57] The proximal iron ($Fe_p$) is directly bonded to the [4Fe-4S] cluster and is coordinatively saturated, whereas the distal iron ($Fe_d$) atom provides a vacant site for substrate binding ($H^+/H_2$), as well as inhibitors (like $O_2$ and CO).[58,59] The crucial enzymatic reaction step is the heterolytic cleavage of $H_2$ into $H^-$ and $H^+$ which is facilitated by an internal base—a pendant amine present in the ADT—that not only captures the proton but also serves as a conduit for proton transfer during catalysis.[53,57,60−64] The iron−sulfur cluster, bound to the proximal iron center, not only regulates electron flow to the catalytic diiron site but also modulates the electrophilicity of the proximal iron center, thus influencing its reactivity.[63,65,66] In contrast, low-valent platinum complexes exhibit a different mode of activation, wherein $H_2$ is homolytically split into two oxidized Pt hydride species. While attempts to replicate the exact structure of the active site of [FeFe]-hydrogenase have fallen short in terms of reactivity, a bioinspired approach has emerged as a promising avenue for the development of catalysts for potential applications in electrolyzers or fuel cells.

In the existing literature, the activation of $H_2$ utilizing synthetic model complexes of hydrogenases is a relatively rare occurrence with only four documented examples. Among these, models featuring a $H_{ox}$ structure incorporating an ADT bridge (Figure 1B) exhibit sluggish reactivity with $H_2$ under high pressure, yielding $\mu$-H complexes.[67] However, in the presence of an additional oxidant, the activation of $H_2$ proceeds more expeditiously under milder conditions.[33] A notable advancement in this field was the development of a functional model of $H_{ox}$ (Figure 1C), incorporating both an internal amine and a redox-active unit, Cp*Fe-($C_5Me_4CH_2PEt_2$) (FcP*) (Cp* = $C_5Me_5$), by the Rauchfuss group.[68] This model demonstrated activity for the oxidation of $H_2$ at 1 atm pressure at 25 °C in the presence of excess $FcBAr^F_4$ [Fc = $Cp_2Fe$, $Ar^F$ = 3,5-$(CF_3)_2C_6H_3$] and P(o-tol)$_3$, achieving a turnover rate of 0.4 per hour over a 5-h period.[68] Subsequently, Sun and colleagues reported another significant advancement, presenting a [FeFe]-hydrogenase model complex (Figure 1D) capable of oxidizing $H_2$ under similar conditions, using excess $Fc^+$ and P(o-tol)$_3$ as oxidant and base, respectively.[69,70] Inspired by the pendant amine present in the ADT bridge of [FeFe]-$H_2$ases, a series of mononuclear nickel complexes based on bis-diphosphine ligands with pendant amines $[Ni(P^R_2N^{R'}_2)_2]^{2+}$ (Figure 1F) (where $P^R_2N^{R'}_2$ is 1,5-R′-3,7-R-1,5-diaza-3,7-diphosphacyclooctane and R and R′ are the alkyl or aryl substituents on P and N atoms) have been reported by DuBois and Shaw,[10,71−73] which can functionally mimic the hydrogenase enzymes where the pendant amine group plays a crucial role by stabilizing the $H_2$ addition with the metal center and facilitating heterolytic cleavage of $H_2$ by proton transportation to or from the metal center as well.[32,73,74] Various substituents (methyl, ethyl, benzyl, phenyl, cyclohexyl, and *tert*-butyl) on P and N atoms were explored, and notably, the complex $[Ni(P^{Cy}_2N^{tBu}_2)_2]^{2+}$ exhibited the highest TOF of 50 $s^{-1}$ for $H_2$ oxidation to date, using $Et_3N$ to scavenge the $H^+$ produced in the process.[75,76] Iron- and ruthenium-based homogeneous electrocatalysts with $P^{tBu}_2N^{Bn}_2$ ligand for hydrogen activation have also been reported with low overpotential values.[36,77] Thus, noble-metal-free alternatives in electrocatalytic hydrogen oxidation are limited to the set of molecular catalysts described above.

We have recently reported a novel group of oxygen-tolerant *ortho*-substituted [FeFe]-hydrogenase model complexes, drawing inspiration from the binuclear ADT-bridged active site of [FeFe]- hydrogenase,[78] which serve as bidirectional catalysts for hydrogen evolution as well as $H_2$ oxidation.[79] These *ortho*-substituted model complexes ($\mu$-$S_2(CH_2)_2NAr$)$[Fe(CO)_3]_2$ (Ar is a 2-Et phenyl group, Figure 1E) exist in a conformation that directs the nitrogen lone pair toward the $H_2$ binding site. The amine group's enhanced basicity relative to unsubstituted analogues, arising from hindered delocalization of the nitrogen lone pair in the aromatic ring, enables efficient hydrogen activation in both organic solvents and heterogeneous conditions, even at a pH of 5.5, with a moderate overpotential (<400 mV).[79] These catalysts are prolific in their application and can be easily integrated with cheap and abundant electrode materials via adsorption.[78,80−82] However, the $H_2$ oxidation rate and activity of these catalysts are low, and more exploration of such catalysts is needed to develop their reactivity.


https://doi.org/10.1021/acsorginorgau.4c00073
ACS Org. Inorg. Au 2025, 5, 105−116

In this report, we have investigated the effect on electrocatalytic homogeneous heterolytic cleavage of hydrogen by introducing electron-withdrawing and electron-donating groups at the *para* position of the *ortho*-substituted arene of the oxygen-tolerant model complex $(\mu\text{-}S_2(CH_2)_2NAr)[Fe(CO)_3]_2$ at various hydrogen concentrations and varying external base ($Et_3N$) concentrations. The results show that under homogeneous conditions, these complexes oxidize $H_2$ with a FY of ∼90% and an overpotential of <480 mV. The substituents on the phenyl ring affect the electronic structure of the diiron cluster, as evident from $^1$H NMR, CV, and FTIR spectroscopy. The complex with an electron-withdrawing group in the secondary coordination sphere demonstrated the highest $H_2$ oxidation rate (2.05 $s^{-1}$), whereas the complex with an electron-donating group exhibited the lowest rate (0.93 $s^{-1}$) under 1 atm of $H_2$.

## RESULTS AND ANALYSIS

### Synthesis and Characterization

Complex **1** was synthesized using a previously reported synthetic protocol.[78] Complexes **2** and **3** were synthesized by following a slightly modified literature procedure.[23,81,83] Typically, combining two equivalents of *p*-formaldehyde with the respective aromatic amines in $CH_2Cl_2$ for 3−4 h followed by the addition of $SOCl_2$ yields the bis-chloromethylated derivative of the same. Subsequent condensation with the $Li_2(\mu\text{-}S)_2[Fe(CO)_3]_2$ salt in dry THF at low temperatures results in the desired complex. For the synthesis of complexes **2** and **3** (**2** = 2-methyl-4-nitroaniline; **3** = 4-methoxy-2-methylaniline), the reaction mixture of *p*-formaldehyde and the respective aromatic amines requires stirring for 48 h (Scheme 1). The synthetic procedures mentioned above are described in detail in the "Experimental Section". All these complexes were characterized using $^1$H NMR (Figures S1−S3), FTIR (Figure 3B), ESI-MS, elemental analysis, and single-crystal X-ray diffraction (SCXRD).

**Scheme 1. General Scheme for the Synthesis of 2-Me-Hyd (1), 2-Me-4-$NO_2$-Hyd (2), and 2-Me-4-OMe-Hyd (3)**

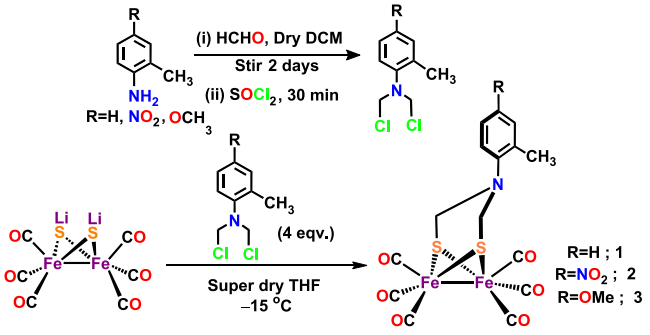


The *ortho* substituent induces rotation of the phenyl ring, thereby diminishing the resonance delocalization of the lone pair of electrons into the phenyl ring. Accordingly, in the $^1$H NMR spectrum of complexes **1**, **2**, and **3** in $CDCl_3$, the $-CH_2-$ resonances are shifted toward higher fields in complex **3** (Figure 3A, green) relative to complex **2** (Figure 3A, blue), with complex **1** (Figure 3A, red) falling in between the two. This shift directly indicates an increase in electron density in the $-CH_2-$ group in complex **3** with the *p*-OMe substituent relative to complex **1**, which has more electron density in the $-CH_2-$ group relative to complex **2** with the *p*-$NO_2$ substituent. This observation suggests that the electron-donating ability of the methoxy (−OMe) group and the electron-withdrawing ability of the nitro ($-NO_2$) group in complexes **3** and **2**, respectively, get translated to the bridging ADT unit. This is also supported by the red-shift in the C−O vibrational frequencies in the FTIR in complex **3** (Figure 3B, green) relative to those in complex **1** (Figure 3B, red), which is, in turn, red-shifted relative to those in complex **2** (Figure 3B, blue), indicating increased electron density into the diiron unit and resulting in enhanced back-bonding in the order **3** > **1** > **2**. High-quality single crystals, characterized by their deep red needlelike appearance, were successfully grown through the gradual evaporation of $CH_2Cl_2$ solutions containing these complexes. The X-ray crystallographic structures of the compounds are depicted in Figure 2. Analysis revealed that the bond lengths of Fe−Fe, Fe−S, and Fe−CO in complexes **1**, **2**, and **3** fall within the range reported for analogous complexes, as detailed in Table 1.[78] The crystal structures of these complexes reveal that the dihedral angles formed by the $C_2$ and $C_1$ carbons of the phenyl ring and the NC bond of the azadithiolate ligand (∠C−C−N−C angle) in complexes **1**, **2**, and **3** are ∼80.92°, ∼54.06°, and ∼74.37°, respectively. These angles are significantly different from those observed in all previously reported N-aryl-substituted ADT structures, where the phenyl plane is nearly coplanar with the $-H_2C-N-CH_2-$ plane of the ADT, showing angles of about 6° and 2.89° in 4-Br-Hyd[81] and 4-$NO_2$-Hyd,[84] respectively.[78] In complexes **1**, **2**, and **3**, the aromatic rings are rotated away from the $-H_2C-N-CH_2-$ plane of the ADT. The three ∠$-H_2C-N-CH_2-$ bond angles are ∼112°, ∼113°, and ∼111°. This indicates that the nitrogen centers in complexes **1**, **2**, and **3** exhibit a tetrahedral geometry, suggesting a $sp^3$ hybridization of the nitrogen. This contrasts with the more planar geometry seen in

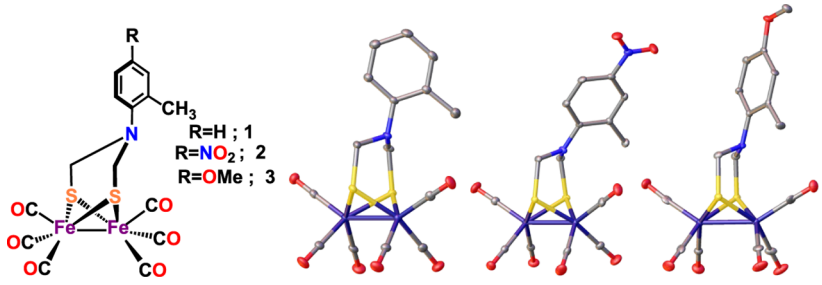


**Figure 2.** Representative structures of the 2Fe subsite mimics of [FeFe]-$H_2$ases and the XRD-determined structures of 2-methyl-, 2-methyl-4-nitro-, and 2-methyl-4-methoxy-substituted phenyl amine containing ADT-bridged 2Fe subsite mimics investigated in this report.


https://doi.org/10.1021/acsorginorgau.4c00073
ACS Org. Inorg. Au 2025, 5, 105−116

**Table 1. Geometric and Spectroscopic Comparison of Complexes 1, 2, and 3 as Determined from X-Ray Crystal Structure**

| Complex | $\nu$ (CO) IR ($cm^{-1}$) | Bonds | Average bond length (Å) | Dihedral angle (∠C−C−N−C) defined by the $C_2C_1$ carbons of the aryl ring and the NC of the ADT ligand |
|---|---|---|---|---|
| 2-Me-Hyd (**1**) | 2073, 2036, 1999 | Fe−Fe | 2.505 (±0.001) | ~80.92° |
| | | Fe−S | 2.246 (±0.001) | |
| | | Fe−CO | 1.801 (±0.001) | |
| 2-Me-4-$NO_2$-Hyd (**2**) | 2075, 2038, 2000 | Fe−Fe | 2.522 (±0.001) | ~54.06° |
| | | Fe−S | 2.235 (±0.001) | |
| | | Fe−CO | 1.799 (±0.001) | |
| 2-Me-4-OMe-Hyd (**3**) | 2072, 2035, 1997 | Fe−Fe | 2.533 (±0.001) | ~74.37° |
| | | Fe−S | 2.253 (±0.001) | |
| | | Fe−CO | 1.802 (±0.001) | |

other N-aryl-substituted complexes and results in an increased basicity of the nitrogen lone pair.

## Electrochemical Investigations

The cyclic voltammetry (CV) of complexes **1**, **2**, and **3** in $CH_3CN$ shows a quasi-reversible redox event at −1.72, −1.63, and −1.77 V vs $Fc^{+/0}$, respectively, characteristic of these clusters (Figure 3C).[25,26,85,86] This process is assigned as a $2e^-$ reduction process [i.e., Fe(I)−Fe(I) + $2e^-$ ⇌ Fe(0)−Fe(0)] and is associated with a substantial change in the geometry of the complex, resulting in the complex nature of the voltammogram.[25,26,86,87] The presence of a redox-active nitro group (−$NO_2$) in complex **2** distinguishes it from complexes **1** and **3**. This difference manifests as an additional reduction peak at −1.79 V observed only in complex **2**. The reduced species generated during the cathodic scan of complexes **1**, **2**, and **3** gets oxidized at −0.74, −0.76, and −0.78 V vs $Fc^{+/0}$, respectively, during the reverse anodic oxidation. The introduction of an electron-withdrawing group (−$NO_2$) on the arene ring of complex **2** (Figure 3C, blue) causes a shift in the reduction potential toward a more anodic value, whereas the incorporation of an electron-donating group (−OMe) on the arene ring of complex **3** (Figure 3C, green) leads to a shift in the reduction potential toward a more cathodic value compared to complex **1** (Figure 3C, red).

## Electrocatalytic Oxidation of Hydrogen

The performance of these newly developed complexes was assessed in terms of their ability to catalyze the oxidation of $H_2$ electrochemically. For catalytic electrochemical measurements, we employed a 1 mM solution of complex **1** dissolved in a 0.1 M $n$$Bu_4NClO_4$ acetonitrile solution. The reaction chamber was maintained at 1 atm of $H_2$, and triethylamine ($Et_3NH^+$, $pK_a$ = 18.8 in $CH_3CN$[88] was added subsequently as a proton scavenger.

Catalytic oxidation of $H_2$ was identified by an increase in the anodic peak current, at the potential where the clusters get oxidized, upon the addition of the exogenous base in the presence of 1 atm $H_2$ (Figure 4A). For complex **1**, the oxidation current initially increases as the concentration of triethylamine is increased until the base concentration reaches 4.3 mM in the presence of 1 atm $H_2$; above this concentration, no significant increase in current is observed as the base concentration is increased to 8.6 mM (Figures 6A and S5). The results for complexes **2** and **3** are quite similar to those found for complex **1** (Figure 4B,C) and will be discussed only briefly.

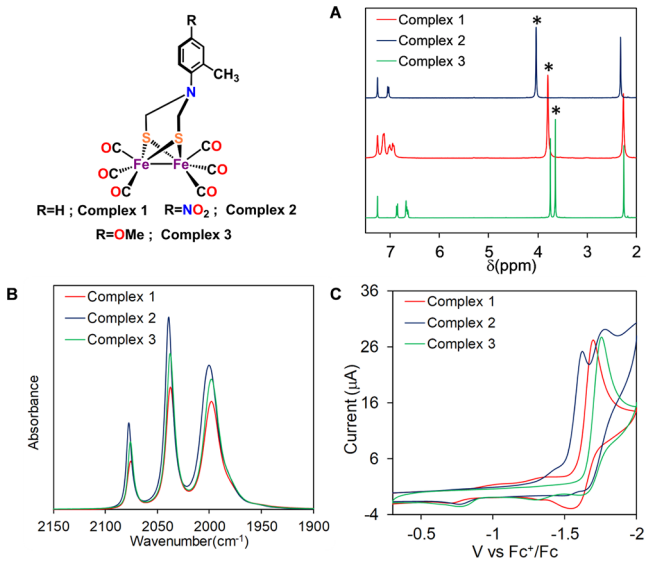


**Figure 3.** (A) Overlay of $^1$H NMR data in $CDCl_3$ of complexes **1**, **2**, and **3**. The $-CH_2-$ resonances are indicated by an asterisk. (B) Overlay of FTIR data of the same complexes in acetonitrile solution. (C) Homogeneous cyclic voltammetry of complexes **1**−**3** in acetonitrile solution under a nitrogen atmosphere (1 mM complex, scan rate 50 mV/s, GC working electrode, and Pt counter electrode, 0.1 M $n$$Bu_4NClO_4$ supporting electrolyte. Potentials are swept from cathodic to anodic direction. Potentials are referenced to $Fc^{+/0}$. This and the following CVs were carried out at room temperature and are reported following the polarographic convention).

The catalytic current became base concentration independent at 5 and 5.7 mM $Et_3N$ concentrations for complexes **2** and **3**, respectively (Figures 6A and S5). The catalytic current became plateau-shaped rather than exhibiting a distinct peak. This behavior is expected for a catalytic wave under conditions where the substrate concentrations (base and $H_2$) are sufficiently high and catalysis is operating in a steady-state kinetic regime. In this regime, factors such as substrate consumption or catalyst deactivation within the electrochemical diffusion layer have minimal influence.[89,90] These findings are consistent with a catalytic process for hydrogen oxidation, and the $H^+$ formed can be estimated from the $Et_3NH^+$ formed in solution during catalysis.[10,36,76,79]

The ratio of $i_{cat}/i_p$ is plotted vs the concentration of triethylamine (where $i_{cat}$ is the catalytic current measured in the presence of base and $H_2$, and $i_p$ is the peak current for the oxidation current of the complexes) (Figure 6A). At low


https://doi.org/10.1021/acsorginorgau.4c00073
ACS Org. Inorg. Au 2025, 5, 105−116

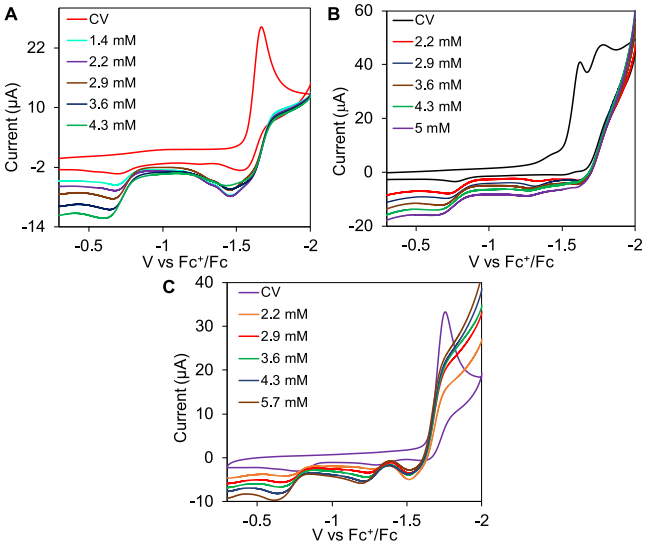


**Figure 4.** Cyclic voltammograms of an acetonitrile solution of (A) complex **1**, (B) complex **2**, and (C) complex **3** and their linear sweep voltammetry under 1.0 atm of $H_2$ with increasing concentrations of triethylamine as indicated in the legend. Conditions: 1 mM catalyst, scan rate 50 mV/s; 0.1 M $n$Bu$_4$NClO$_4$ as supporting electrolyte; glassy carbon working electrode; Pt counter electrode. Potentials are swept from the cathodic to anodic direction. Potentials are referenced to $Fc^{+/0}$. These CVs were carried out at room temperature and are reported following the polarographic convention.

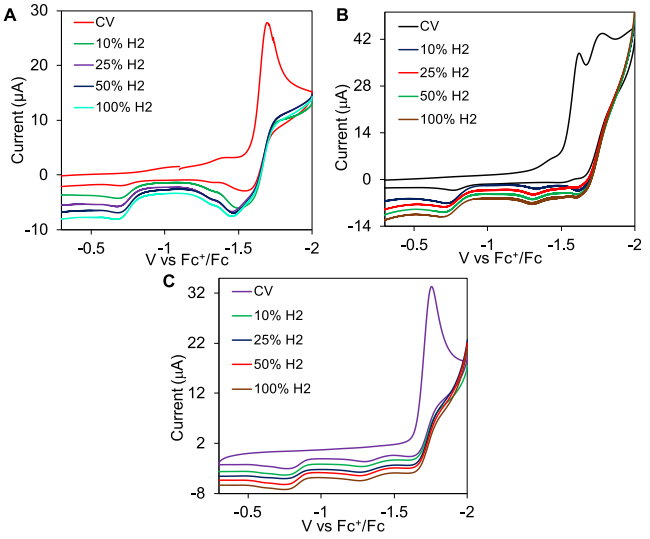


**Figure 5.** Cyclic voltammograms of an acetonitrile solution of (A) complex **1**, (B) complex **2**, and (C) complex **3** and their linear sweep voltammetry in the presence of 4.3 mM $Et_3N$ at different $H_2$ concentrations as indicated in the legend. Conditions: 1 mM catalyst, scan rate 50 mV/s; 0.1 M $n$Bu$_4$NClO$_4$ as supporting electrolyte; glassy carbon working electrode; and Pt counter electrode. Potentials are swept from the cathodic to anodic direction. Potentials are referenced to $Fc^{+/0}$. These CVs were carried out at room temperature and are reported following the polarographic convention.

concentrations of the base, the ratio of $i_{cat}/i_p$ shows a linear relationship with the square root of base concentration, indicating that the catalytic rate is first-order with respect to base concentration (Figure 6B).[36,91,92] The catalytic current also increases linearly with the square root of the partial pressure of $H_2$, consistent with a first-order dependence of the homogeneous catalytic process on $H_2$ (Figures 5 and 66C).[10,79,93] Using a constant base concentration under 1 atm of $H_2$, the observed catalytic current ($i_{cat}$) increases linearly as a function of catalyst concentration, indicating that the reaction is first-order in catalyst concentration (Figure S6).[10,36] Control experiments with triethylamine/$H_2$, but no catalysts, show no significant current (Figure S9). Also, in the absence of $H_2$, the subsequent addition of triethylamine into the complex solution displays no significant increment of current (Figure S10).

Calculation of $k_{obs}$ was only performed after the base-independent current had been achieved (i.e., a pseudo-zero-order kinetics with respect to base concentration had been reached). The $i_{cat}/i_p$ ratio becomes independent of the base concentration at higher concentrations of base, with a maximum $i_{cat}/i_p$ ratio of 3.71 at a scan rate of 50 mV s$^{-1}$ for complex **1** under 1 atm of $H_2$. For complexes **2** and **3**, the maximum $i_{cat}/i_p$ ratio is calculated to be 4.6 and 3.1, respectively, under similar conditions. This $i_{cat}/i_p$ value can be used to calculate a pseudo-first-order rate ($k_{obs}$) or turnover frequency (TOF, in units of ((mol of $H_2$)/s)/(mol of catalyst)), for $H_2$ oxidation under 1.0 atm $H_2$, as shown in eq 3,[89,90,94,95] where $n$ is the number of electrons (2 for $H_2$ oxidation), R is the universal gas constant (8.314 J K$^{-1}$ mol$^{-1}$), F is Faraday's constant (9.65 × 10$^4$ C mol$^{-1}$), $T$ is the temperature in Kelvin, $\nu$ is the scan rate in V s$^{-1}$, and 0.4463 is a constant determined by numerical solution of the diffusion equations.[90] Using the maximum $i_{cat}/i_p$ ratio in eq 3 under the

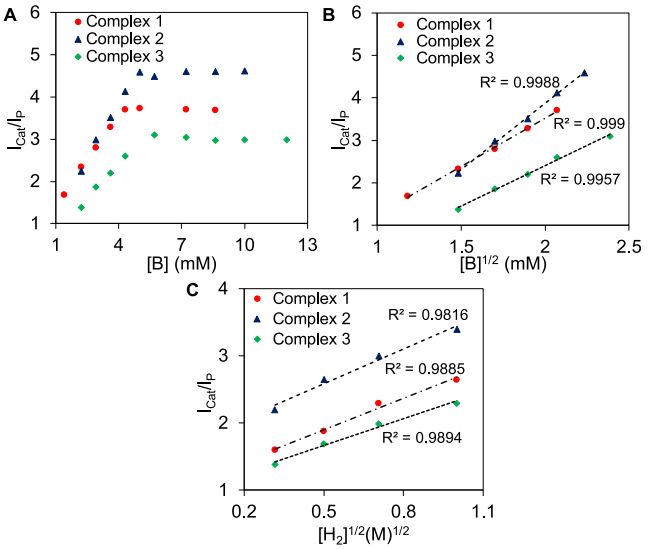


**Figure 6.** (A) Plot of $i_{cat}/i_p$ vs [$Et_3N$] for the oxidation of $H_2$ by a 1 mM solution of complexes **1**, **2**, and **3** in acetonitrile under 1 atm of $H_2$. (B) Plot of $i_{cat}/i_p$ vs the square root of base concentration ($Et_3N$) for a 1.0 mM solution of complexes **1**, **2**, and **3** under lower base concentrations (under 1.0 atm $H_2$, 50 mV/s scan rate). (C) Plot of $i_{cat}/i_p$ vs the square root of the partial pressure of $H_2$ in the presence of 4.3 mM of $Et_3N$ (scan rate = 50 mV/s). Conditions: 0.1 M $n$Bu$_4$NClO$_4$ as supporting electrolyte and glassy carbon working electrode.

base-independent region, the turnover frequencies (TOFs) are calculated to be 1.33, 2.05, and 0.93 s$^{-1}$ for complexes **1**, **2**, and **3**, respectively, under 1 atm of $H_2$ (Table 2).

$$\frac{i_{cat}}{i_p} = \frac{n}{0.4463}\sqrt{\frac{RTk_{obs}}{F\nu}}$$



https://doi.org/10.1021/acsorginorgau.4c00073
ACS Org. Inorg. Au 2025, 5, 105−116

$$\mathrm{TOF} = k_{\mathrm{obs}} = \frac{0.1992\mathrm{F}\nu}{n^2\mathrm{R}T}\left(\frac{i_{\mathrm{cat}}}{i_{\mathrm{p}}}\right)^2 \quad (3)$$

**Table 2. Electrocatalytic Data for Hydrogen Oxidation by Complexes 1, 2, and 3 under 1 atm $H_2$ in 0.1 M [$n$Bu$_4$NClO$_4$]-CH$_3$CN**

| Complex | $E_{cat/2}$ (mV vs. $Fc^{+/0}$) | Overpotential (mV vs $Fc^{+/0}$) | $k_{obs}$ ($s^{-1}$) | % FY |
|---|---|---|---|---|
| 2-Me-Hyd (**1**) | −740 | 440 | 1.33 ± 0.02 | 88 |
| 2-Me-4-$NO_2$-Hyd (**2**) | −780 | 400 | 2.05 ± 0.02 | 92 |
| 2-Me-4-OMe-Hyd (**3**) | −700 | 480 | 0.93 ± 0.02 | 90 |

The half-wave potential for the catalytic process, $E_{cat/2}$, was defined at half of the catalytic current. The electrocatalytic HOR process mediated by complex **1** has a half-peak potential of −740 mV vs $Fc^{+/0}$. The apparent standard potential of $H_2$ oxidation in $CH_3CN$ is −1.18 V vs $Fc^{+/0}$ using 18.8 as the p$K_a$ value of $Et_3N$ in acetonitrile and −0.07 V vs $Fc^{+/0}$ as the thermodynamic proton reduction potential value.[79,96,97] This indicates that the overpotential requirement for HOR catalyzed by complex **1** is ∼440 mV in acetonitrile solution. Similarly, the overpotentials for HOR catalyzed by complexes **2** and **3** are calculated to be ∼400 and ∼480 mV, respectively. This value compares well with the HOR overpotential displayed in acetonitrile by most DuBois' catalysts.[10,76]

The proton generated from the oxidation of $H_2$ is converted to the $Et_3NH^+$ cation. Quantification of the $Et_3NH^+$ cation by $^1$H NMR during the course of a bulk electrolysis (BE) experiment under stirring conditions is carried out in a 0.5 mM $CD_3CN$ solution (8 mL) of the catalyst in the presence of an excess of $Et_3N$ (50 mM) at −0.7 V vs $Fc^{+/0}$ under 1 atm of hydrogen (Figure S15).[79] As shown in Figure S18, in the presence of $Et_3N$, the electrolysis of complex **1** under a $H_2$ atmosphere resulted in a new peak appeared at 7.95 ppm, which can be attributed to $Et_3NH^+$. Quantification of the $Et_3NH^+$ signal and its ratio with the charge consumed yields the FY to be ∼88% for complex **1**, ∼92% for complex **2**, and ∼90% for complex **3**.

The decay of the catalyst is calculated to be ∼12−15% (∼15% for complex **1**, ∼12% for complex **2**, and ∼14% for complex **3**) from the UV−visible spectra of the catalyst before and after long-term bulk electrolysis (Figure S17). Moreover, after an electrochemical measurement of the complexes, a subsequent CV measurement of the glassy carbon electrode under the same conditions did not show any catalytic behavior distinct from that of the glassy carbon electrode (Figure S16), indicating that no deposit is formed on the electrode, and these catalysts are stable during electrochemical measurements. To check the background $H_2$ oxidation on the electrode, a control bulk electrolysis experiment was performed without a catalyst in the presence of excess triethylamine ($Et_3N$) and 1 atm of hydrogen ($H_2$) in the $CD_3CN$ solvent. $^1$H NMR analysis in $CD_3CN$ showed no significant formation of triethylammonium ($Et_3NH^+$) during electrolysis (Figure S21).

## Mechanism of $H_2$ Oxidation

The mechanism of $H_2$ oxidation was proposed to involve $H_2$ binding to the Fe(I)−Fe(I) state of this class of complexes, and this step was computed to be endothermic and likely the rate-determining step in catalysis.[79] The reduction of such diiron hexacarbonyl clusters is irreversible, and it has been proposed that the reduction may lead to changes in the cluster geometry.[98,99] To confirm if the reoxidation peaks observed around −0.8 V are likely due to the oxidation of the daughter products of reduced complexes **1**, **2**, and **3**, rather than the oxidation of the parent complexes, we performed $H_2$ oxidation of complex **3** using different initial potentials (Figure 7A). The

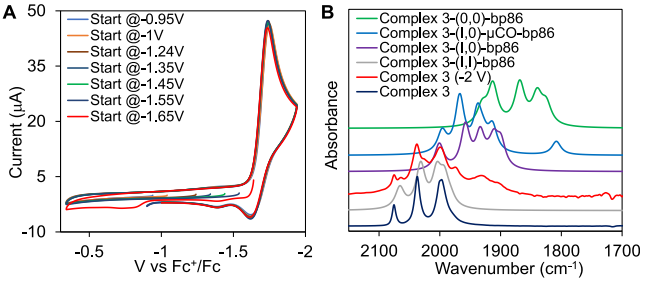


**Figure 7.** (A) Cyclic voltammograms of an acetonitrile solution of complex **3** starting from different potentials as indicated in the legend in the presence of 2 mM of $Et_3N$ under 1 atm of $H_2$. Conditions: scan rate 50 mV/s, 1 mM complex; 0.1 M $n$Bu$_4$NClO$_4$ as supporting electrolyte; glassy carbon working electrode; Pt counter electrode. Potentials are referenced to $Fc^{+/0}$. (B) Experimental FTIR data (dark blue), FTIR SEC data (red), and computed vibrations (for singly and doubly reduced states) of complex **3**.

experimental data show that indeed a $H_2$ oxidation current is observed when the initial potential is lowered below the onset of the two-electron reduction process of the Fe (I)−Fe(I) state (Figure 7A). This clearly indicates that the species produced during reduction, which gets reoxidized at −0.78 V vs $Fc^{+/0}$, is likely the catalyst responsible for $H_2$ oxidation. Additionally, CV of complex **3** at different scan rates reveals that indeed there is a change in the geometry of the cluster upon reduction, which results in two closely spaced pairs of anodic oxidations centered around −1.3 V vs $Fc^{+/0}$ and −0.78 V vs $Fc^{+/0}$ at slow scan rates (Figure S12A). At higher scan rates, the CV becomes quasi-reversible, and the process at −0.78 V vs $Fc^{+/0}$ reduces, indicating that the change in geometry upon reduction is slow (Figure S12B). This raises the possibility that $H_2$ oxidation during electrolysis is catalyzed by the species produced upon reduction of the cluster.

To investigate the reduction of complex **3**, FTIR spectroelectrochemistry (FTIR-SEC) is performed. We subjected the acetonitrile solution of complex **3** to electrochemical reduction by performing controlled potential electrochemistry (CPE) at −2 V vs $Fc^{+/0}$, within a conventional OTTLE cell to probe the reduced species. Reduction of complex **3** results in a red-shift in the $\nu_{CO}$ vibrations (Figure 7, red) as would be expected for a reduction event in the cluster, which would have increased back-bonding to carbonyl ligands. Upon reduction, the three $\nu_{CO}$ vibrations of complex **3** (2072, 2035, and 1997 $cm^{-1}$) red-shifted to 1973, 1928, and 1903 $cm^{-1}$ (Figure 7B, red). DFT calculations, which reproduce the experimental FTIR spectra of complex **3** (Figure 7B, dark blue vs gray), are used to compute the predicted spectra of the Fe (I)−Fe(0) state (Figure 7B, purple) and the Fe (0)−Fe(0) state (Figure 7B, green) with the same geometry and the Fe(I)−Fe(0) state with a $\mu$-CO ligand (Figure 7B, blue). The calculated $\mu$-CO vibration for the Fe(I)−Fe(0)−$\mu$-CO complex appears at 1804 $cm^{-1}$, which does not align with the experimental data. Therefore, this possibility can be ruled out. The experimentally


https://doi.org/10.1021/acsorginorgau.4c00073
ACS Org. Inorg. Au 2025, 5, 105−116

observed $\nu_{CO}$ around 1900 $cm^{-1}$ falls in the region predicted for the Fe(I)−Fe(0) state by DFT calculations. However, the FTIR spectra are complicated by the fact that there is still substantial intensity in the region where the Fe(I)−Fe(I) state absorbed, and this either could be the original Fe(I)−Fe(I) species not yet electrolyzed or may represent the absorption from one of the reduced daughter species formed where a bridging thiolate dissociates. At this point, it is unclear what the nature of the active species is, and further investigations are needed to identify the species responsible for $H_2$ oxidation by these bioinspired models of [FeFe]-$H_2$ase.

## SUMMARY

The activation of $H_2$ by diiron models necessitates that the catalytically active iron center be adequately electrophilic to bind $H_2$, while also being insufficiently electrophilic to prevent the amine from binding to the Fe.[100] Both the active site of classical [FeFe]-hydrogenases and the ferrocene-bearing diiron mimic ($FcFe_2$, Figure 1C) reported by Rauchfuss and coworkers react with $H_2$ in the Fe(II)−Fe(I) state.[35] Such a deviation of the reactivity relative to the electronic structure is due to the difference in the ligand environments in these systems. In the natural active site, a $-CN^-$ ligand and a thioether ligand replace two $\pi$-acidic −CO ligands in complexes **1**, **2**, and **3**, resulting in increased electron density of the diiron cluster. The same is true for the $FcFe_2$ complex, where the diphosphine ligand replaces the two $\pi$-acidic −CO ligands in these complexes. This is why the Fe(II)−Fe(I) mixed-valent state is required to oxidize $H_2$ in the enzyme active site and $FcFe_2$ complex (Figure 1C), while the Fe(I)−Fe(I) state of the daughter species produced upon two-electron reduction of complexes **1**, **2**, and **3** can react with $H_2$, albeit the structure of this species is yet to be elucidated. The systematic variation of the rate of HOR with the ring substituent suggests that the catalytically active species retain the ADT ligand, and its electronic structure is affected by the substitutions on the ADT ligand. These are crucial hints for the determination of the structure of the catalyst responsible for $H_2$ oxidation. Taken together, these data suggest that the presence of an electron-withdrawing $-NO_2$ group in complex **2** within the second coordination sphere facilitates the rate-limiting $H_2$ binding step by withdrawing electron density, rendering the iron center of these daughter species sufficiently electrophilic to bind $H_2$. Consequently, its rate of HOR is accelerated compared to complex **3**, which features an electron-donating −OMe group in the second coordination sphere. The results presented here indicate that the substitution of the aryl amine group of the ADT bridge is a viable strategy to improve the HOR catalysis in these groups of complexes.

## EXPERIMENTAL SECTION

### General Information

Complex **1** was synthesized according to the previously reported procedure.[78] Syntheses of all the compounds were performed either under an anaerobic atmosphere or in an Ar glovebox from MBRAUN. Complexes **2** and **3** were synthesized using standard Schlenk techniques.[78] 2-Methylaniline, 4-methoxy-2-methylaniline, and the solvents were used fresh after distillation, purchased from Merck. Thionyl chloride ($SOCl_2$) was purchased from Spectrochem Pvt. Ltd. 2-Methyl-4-nitroaniline, *p*-formaldehyde, superhydride (Li[$HBEt_3$], 1 M in THF), triethylamine, tetrabutylammonium perchlorate (TBAP), and bis(cyclopentadienyl)cobalt(II) were from Sigma-Aldrich Chemicals Pvt. Ltd., and anhydrous $Na_2SO_4$ was purchased from Merck Specialties Pvt. Ltd. (India). Silica (60−120 mesh), for column chromatography, was purchased from SISCO Pvt. Ltd. (India). Ultrahigh purity $N_2$ and $H_2$ cylinders were purchased from Indian Refrigeration Stores. During electrochemistry, the solvent (acetonitrile) was used after distillation with a proper drying agent. The glassy carbon plate (1 mm thick, type 1) was purchased from Alfa Aesar. The FTIR data were measured on the PerkinElmer FTIR Frontier instrument. The $CaF_2$ windows for FTIR spectroscopy were purchased from Sigma-Aldrich. The anaerobic setup for FTIR spectroscopy was purchased from PerkinElmer. The optically transparent thin-layer electrochemical (OTTLE) cell was purchased from the University of Reading for spectroelectrochemistry. All of the NMR spectra were recorded on Bruker DPX-400 and DPX-500 spectrometers at room temperature. UV−vis absorption data were recorded in an Agilent Technologies model 8453 spectrophotometer fitted with a diode-array detector. All the NMR spectra were recorded on a Bruker DPX-400 or DPX-500 spectrometer at room temperature. The mass spectra were recorded on a QTOF MicroYA263 instrument.

### General Procedures for Synthesis

Complex **1**, $[(\mu\text{-}SCH_2)_2N(2\text{-Methylphenyl})CH_2S)[Fe(CO)_3]_2$. Complex **1** was synthesized by a previously reported procedure.[78] $^1H$ NMR (500 MHz, $CDCl_3$) $\delta$ 7.14 (d, $J$ = 7.4 Hz, 2H), 7.01 (s, 1H), 6.95 (s, 1H), 3.79 (s, 4H), 2.13 (s, 3H). IR ($CH_3CN$): 2073 $cm^{-1}$(s), 2036 $cm^{-1}$(s), 1999 $cm^{-1}$(s). HRMS (ESI-TOF) $m/z$: $(M+H)^+$ Calcd for $C_{15}H_{11}Fe_2NO_6S_2H$ 477.0640; Found 477.0742. Elemental Analysis (found): C, 37.34; H, 3.79; N, 2.42; calculated C, 37.29; H, 3.55; N, 2.90.

Complex **2**, $[(\mu\text{-}SCH_2)_2N(2\text{-Methyl-4-nitrophenyl})\ CH_2S)\ [Fe(CO)_3]_2$. Complex **2** was synthesized using standard Schlenk techniques by slightly modifying the synthetic protocol described in the literature.[83] To a solution of 2-methyl-4-nitroaniline (1.52 g, 10 mmol) was added paraformaldehyde (780 mg, 26 mmol); the solution was stirred for 2 days at room temperature. Then, $SOCl_2$ was slowly added at 0 °C, and the mixture was brought to RT with stirring. After 0.5 h, the solvent was evaporated completely to dryness to remove all the acid vapor. A 440 mg sample of $(\mu\text{-}S_2)[Fe(CO)_3]_2$ (1 mmol) was dissolved in 20 mL of dry tetrahydrofuran (THF). Two milliliters of $LiBEt_3H$ (1 M in THF) were added dropwise to the red solution at −78 °C, with an immediate color change to deep green. Following cooling to −15 °C, a THF solution of the ligand 2-$CH_3$-4-$NO_2$−$C_6H_4N(CH_2)_2Cl_2$ (4 equiv) was added to the reaction mixture. The color immediately changed to red. The reaction mixture was further stirred for 1 h at RT. Vacuum removal of the solvent produced a dark brown precipitate. A crystalline red solid product was obtained after column chromatography with a hexane−toluene (9:1) mixture. Reddish-brown single crystals were grown by the slow evaporation of a $CH_2Cl_2$ solution of the complex. Overall yield: 45% (58 mg). $^1H$ NMR ($CDCl_3$, 400 MHz): $\delta$ 8.04 (d, $J$ = 12.2 Hz, 2H), 7.04 (d, $J$ = 8.8 Hz, 1H), 4.03 (s, 4H), 2.32 (s, 3H). IR ($CH_3CN$): 2075 $cm^{-1}$(s), 2038 $cm^{-1}$(s), 2000 $cm^{-1}$(s). HRMS (ESI-TOF) $m/z$: $(M+H)^+$ Calcd for $C_{15}H_{10}Fe_2N_2O_8S_2H$ 522.8577; Found 522.8599. Elemental Analysis (found): C, 34.48; H, 1.90; N, 5.35; calculated C, 34.51; H, 1.93; N, 5.37.

Complex **3**, $[(\mu\text{-}SCH_2)_2N(2\text{-Methyl-4-methoxy})CH_2S)[Fe(CO)_3]_2$. Complex **3** was synthesized following the exact same procedure described for complex **2**, using 4-methoxy-2-methylaniline (1.37 mL, 10 mmol) instead of 2-methyl-4-nitroaniline. The column chromatography was performed using a hexane−toluene (9:1) mixture to yield a crystalline reddish-brown solid. Suitable single crystals were obtained by the slow evaporation of a $CH_2Cl_2$ solution of the complex. Overall yield: 44% (52 mg). $^1H$ NMR ($CDCl_3$, 400 MHz): $\delta$ 6.86 (d, $J$ = 8.6 Hz, 1H), 6.74−6.57 (m, 2H), 3.75 (s, 3H), 3.64 (s, 4H), 2.25 (s, 3H). IR ($CH_3CN$): 2072 $cm^{-1}$(s), 2035 $cm^{-1}$(s), and 1997 $cm^{-1}$(s). HRMS (ESI-TOF) $m/z$: $(M+H)^+$ Calcd for $C_{16}H_{13}Fe_2NO_7S_2H$ 507.8832; Found 507.8854. Elemental Analysis (found): C, 37.85; H, 2.60; N, 2.78; calculated C, 37.90; H, 2.58; N, 2.76.


https://doi.org/10.1021/acsorginorgau.4c00073
ACS Org. Inorg. Au 2025, 5, 105−116

**Electrochemical Measurements.** All the electrochemical measurements were carried out in dry, degassed $CH_3CN$ solution (Merck, HPLC gradient grade 99.99%), 0.1 M $n$Bu$_4$NClO$_4$ (Sigma-Aldrich, for electrochemical analysis ≥99%, used as received), under a nitrogen or hydrogen atmosphere, where indicated, at room temperature using a CH Instruments (model CHI 700E electrochemical analyzer). For CV experiments, a four-neck custom-made electrochemical cell was used. Potentials were referred to an Ag/AgCl (saturated KCl) reference electrode in $CH_3CN$ + 0.1 M $n$Bu$_4$NClO$_4$, and measured potentials were calibrated through the use of an internal $Fc^{+/0}$ standard. A glassy carbon electrode (CV, LSV) and a glassy carbon plate electrode (CPE) were used as working electrodes. The auxiliary electrode was a Pt wire in a $CH_3CN$ + 0.1 M $n$Bu$_4$NClO$_4$ solution. Between CV scans, the working electrode was polished in a figure-eight pattern with an alumina slurry (0.05 $\mu$m) on a micro-cloth (2.875 in, PSA backed). Bulk electrolysis and coulometry were carried out in a four-neck custom-made electrochemical cell using a glassy carbon plate electrode under stirring conditions. The reference electrode was externally calibrated vs $Fc^{+/0}$. The electrolysis was performed after saturating the acetonitrile solution with $H_2$ gas (45 min of purging).

**$H_2$ Concentration Dependence Using a Mass Flow Meter.** The $H_2$ concentration dependence experiments were performed by using a CVG Technocrafts India mass flow meter purchased from Chemix. The mass flow rates of the gases were controlled manually during the experiments using a regulator. In this experiment, we used two different flow meters with a full setup (one for $H_2$ gas control and another for argon gas control). The outlets from these two flow meters were put into a closed vessel through a rubber septum in which two gases were mixed to form a homogeneous gas mixture. Another outlet of this closed vessel was connected to the electrochemical cell. During the $H_2$ concentration dependence experiment, different types of $H_2$/Ar gas mixtures were used. During the experiments, each time, the gas mixture was purged for 45 min into the solution, and then, the data were recorded.

**Bulk Electrolysis and NMR Spectroscopy.** The BE experiment was done in a custom-made four-neck electrochemical cell with a glassy carbon (2 × 2.25 cm$^2$) working electrode under stirring conditions. After saturating the acetonitrile-$d_3$ ($CD_3CN$) solution (containing 0.5 mM complex **1** and 50 mM triethylamine) with $H_2$ gas for 45 min, the BE experiment was performed. During CPE at first, the potential was held at −1.68 V for 60 min, and after that, the CPE was performed at −0.7 V for 9 h, under stirring conditions. The amount of ammonium produced was quantified from the integration values of the new peak, which is generated at 7.95 ppm. We consider the integration of the $-CH_2-$ peak of the complexes as 1.

The faradaic yield (FY) was determined by eq :4

$$\begin{aligned} \mathrm{FY} &= 2 \times \text{amount of ammonium measured}/(\text{charge}/F) \\ &= 2 \times \text{amount of ammonium measured}/\text{charge} \end{aligned} \quad (4)$$

**X-Ray Structure Determinations.** X-ray data were collected either at 150 K on a Bruker SMART APEX-II diffractometer with graphite-monochromated Mo K$\alpha$ radiation ($\lambda$ = 0.71073 Å) controlled by the APEX2 (v.2010.1−2) software package (complex **1**) or at 100 K on a Bruker D8 VENTURE Microfocus diffractometer equipped with a PHOTON II Detector, with Mo K$\alpha$ radiation ($\lambda$ = 0.71073 Å), controlled by the APEX3 (v.2017.3−0) software package (complexes **2** and **3**). Raw data were integrated and corrected for Lorentz and polarization effects by using the Bruker APEX II/APEX III program suite. Absorption corrections were performed using SADABS. Space groups were assigned by analysis of metric symmetry and systematic absences (determined by XPREP) and were further checked by PLATON[101,102] for additional symmetry. All the structures were solved by direct methods and were refined against all data in the reported 2$\theta$ ranges by full-matrix least-squares on $F^2$ with the SHELXL program suite[103] using the OLEX 2 interface.[104] Hydrogen atoms at idealized positions were included during the final refinements of each structure. The OLEX 2 interface was used for structure visualization, analysis of bond distances and angles, and drawing of ORTEP plots.

### Computational Details

The geometries were optimized in Gaussian 16 software[105] using the BP86 functional,[106,107] 6-311g* basis set, and PCM-dispersion model. Frequency calculations were performed on each optimized structure using the same basis set to ensure that there was a minimum on the potential energy surface. The single-point calculations were calculated using the same functional but a 6-311+g* basis set and $10^{-10}$ Hartree convergence criteria. Basis-set superposition error has been reported to be minimal (≈1 kcal/mol) for anion binding at this level of theory.

## ■ ASSOCIATED CONTENT

### Data Availability Statement

The data underlying this study are available in the published article and its Supporting Information.

### Supporting Information

The Supporting Information is available free of charge at https://pubs.acs.org/doi/10.1021/acsorginorgau.4c00073.

Additional experimental data, NMR data, and crystallographic data (PDF)

### Accession Codes

CCDC 2332582, 2332584 contain the supplementary crystallographic data for this paper. These data can be obtained free of charge via www.ccdc.cam.ac.uk/data_request/cif, or by emailing data_request@ccdc.cam.ac.uk, or by contacting The Cambridge Crystallographic Data Centre, 12 Union Road, Cambridge CB2 1EZ, UK; fax: + 44 1223 336033.

## ■ AUTHOR INFORMATION


### Corresponding Authors

**Somdatta Ghosh Dey** − *School of Chemical Science, Indian Association for the Cultivation of Science, Kolkata, West Bengal 700032, India;* orcid.org/0000-0002-6142-2202; Email: somdattaghoshdey@gmail.com

**Abhishek Dey** − *School of Chemical Science, Indian Association for the Cultivation of Science, Kolkata, West Bengal 700032, India;* orcid.org/0000-0002-9166-3349; Email: abbeyde@gmail.com

### Authors

**Abhijit Nayek** − *School of Chemical Science, Indian Association for the Cultivation of Science, Kolkata, West Bengal 700032, India;* orcid.org/0000-0001-9981-4271

**Rabin Kumar Poria** − *School of Chemical Science, Indian Association for the Cultivation of Science, Kolkata, West Bengal 700032, India;* orcid.org/0009-0009-7507-2352

**Md Estak Ahmed** − *School of Chemical Science, Indian Association for the Cultivation of Science, Kolkata, West Bengal 700032, India;* orcid.org/0000-0002-0817-2099

**Suman Patra** − *School of Chemical Science, Indian Association for the Cultivation of Science, Kolkata, West Bengal 700032, India;* orcid.org/0000-0003-4572-614X

Complete contact information is available at: https://pubs.acs.org/10.1021/acsorginorgau.4c00073


### Author Contributions

A.N.: conceptualization, data curation, formal analysis, investigation, methodology, and writing—original draft; R.K.P.: data curation and formal analysis; M.E.A.: formal



https://doi.org/10.1021/acsorginorgau.4c00073
ACS Org. Inorg. Au 2025, 5, 105−116

analysis; S.P.: formal analysis; S.G.D.: formal analysis, funding acquisition, project administration, and supervision; A.D.: conceptualization, formal analysis, funding acquisition, methodology, project administration, supervision, and writing—review and editing.

### Funding

This research was supported by the Department of Science and Technology, India, by grant DST/TMD/HFC/2K18/90.

### Notes

The authors declare no competing financial interest.

## ■ ACKNOWLEDGMENTS

A.N. acknowledges IACS for the fellowship. R.K.P. and S.P. acknowledge UGC-JRF and CSIR-SRF, respectively, for the fellowship.

## ■ REFERENCES

(1) Lewis, N. S.; Nocera, D. G. Powering the Planet: Chemical Challenges in Solar Energy Utilization. *Proc. Natl. Acad. Sci. U. S. A.* **2006**, *103* (43), 15729−15735.
(2) Cook, T. R.; Dogutan, D. K.; Reece, S. Y.; Surendranath, Y.; Teets, T. S.; Nocera, D. G. Solar Energy Supply and Storage for the Legacy and Nonlegacy Worlds. *Chem. Rev.* **2010**, *110* (11), 6474−6502.
(3) Yan, Z.; Hitt, J. L.; Turner, J. A.; Mallouk, T. E. Renewable Electricity Storage Using Electrolysis. *Proc. Natl. Acad. Sci. U. S. A.* **2020**, *117* (23), 12558−12563.
(4) Saikia, K.; Kakati, B. K.; Boro, B.; Verma, A. Current Advances and Applications of Fuel Cell Technologies BT. In *Recent Advancements in Biofuels and Bioenergy Utilization*. Sarangi, P. K.; Nanda, S.; Mohanty, P., Ed.; Springer: Singapore, 2018; pp. 303−337.
(5) Winter, M.; Brodd, R. J. What Are Batteries, Fuel Cells, and Supercapacitors? *Chem. Rev.* **2004**, *104* (10), 4245−4270.
(6) Bullock, R. M.; Chen, J. G.; Gagliardi, L.; Chirik, P. J.; Farha, O. K.; Hendon, C. H.; Jones, C. W.; Keith, J. A.; Klosin, J.; Minteer, S. D.; et al. Using Nature's Blueprint to Expand Catalysis with Earth-Abundant Metals. *Science* **2020**, *369* (6505), No. eabc3183.
(7) Wang, M.; Chen, L.; Sun, L. Recent Progress in Electrochemical Hydrogen Production with Earth-Abundant Metal Complexes as Catalysts. *Energy Environ. Sci.* **2012**, *5* (5), 6763−6778.
(8) Thoi, V. S.; Sun, Y.; Long, J. R.; Chang, C. J. Complexes of Earth-Abundant Metals for Catalytic Electrochemical Hydrogen Generation under Aqueous Conditions. *Chem. Soc. Rev.* **2013**, *42* (6), 2388−2400.
(9) Ralph, T. R.; Hogarth, M. P. Catalysis for Low Temperature Fuel Cells. *Platinum Met. Rev.* **2002**, *46* (3), 117−135.
(10) Wilson, A. D.; Newell, R. H.; McNevin, M. J.; Muckerman, J. T.; Rakowski DuBois, M.; DuBois, D. L. Hydrogen Oxidation and Production Using Nickel-Based Molecular Catalysts with Positioned Proton Relays. *J. Am. Chem. Soc.* **2006**, *128* (1), 358−366.
(11) Wilson, A. D.; Shoemaker, R. K.; Miedaner, A.; Muckerman, J. T.; DuBois, D. L.; DuBois, M. R. Nature of Hydrogen Interactions with Ni(II) Complexes Containing Cyclic Phosphine Ligands with Pendant Nitrogen Bases. *Proc. Natl. Acad. Sci. U. S. A.* **2007**, *104* (17), 6951−6956.
(12) Fraze, K.; Wilson, A. D.; Appel, A. M.; Rakowski DuBois, M.; DuBois, D. L. Thermodynamic Properties of the Ni−H Bond in Complexes of the Type [HNi(P2RN2R′)2](BF4) and Evaluation of Factors That Control Catalytic Activity for Hydrogen Oxidation/Production. *Organometallics* **2007**, *26* (16), 3918−3924.
(13) Appel, A. M.; Pool, D. H.; O'Hagan, M.; Shaw, W. J.; Yang, J. Y.; Rakowski DuBois, M.; DuBois, D. L.; Bullock, R. M. [Ni(PPh2NBn2)2(CH3CN)]2+ as an Electrocatalyst for H2 Production: Dependence on Acid Strength and Isomer Distribution. *ACS Catal.* **2011**, *1* (7), 777−785.
(14) Helm, M. L.; Stewart, M. P.; Bullock, R. M.; DuBois, M. R.; DuBois, D. L. A Synthetic Nickel Electrocatalyst with a Turnover Frequency above 100,000 $S^{-1}$ for $H_2$ Production. *Science* **2011**, *333* (6044), 863−866.
(15) Kilgore, U. J.; Stewart, M. P.; Helm, M. L.; Dougherty, W. G.; Kassel, W. S.; DuBois, M. R.; DuBois, D. L.; Bullock, R. M. Studies of a Series of [Ni(PR2NPh2)2(CH3CN)]2+ Complexes as Electrocatalysts for H2 Production: Substituent Variation at the Phosphorus Atom of the P2N2 Ligand. *Inorg. Chem.* **2011**, *50* (21), 10908−10918.
(16) Wilson, A. D.; Fraze, K.; Twamley, B.; Miller, S. M.; DuBois, D. L.; Rakowski DuBois, M. The Role of the Second Coordination Sphere of [Ni(PCy2NBz2)2](BF4)2 in Reversible Carbon Monoxide Binding. *J. Am. Chem. Soc.* **2008**, *130* (3), 1061−1068.
(17) Jacobsen, G. M.; Yang, J. Y.; Twamley, B.; Wilson, A. D.; Bullock, R. M.; Rakowski DuBois, M.; DuBois, D. L. Hydrogen Production Using Cobalt-Based Molecular Catalysts Containing a Proton Relay in the Second Coordination Sphere. *Energy Environ. Sci.* **2008**, *1* (1), 167−174.
(18) Wiedner, E. S.; Yang, J. Y.; Dougherty, W. G.; Kassel, W. S.; Bullock, R. M.; DuBois, M. R.; DuBois, D. L. Comparison of Cobalt and Nickel Complexes with Sterically Demanding Cyclic Diphosphine Ligands: Electrocatalytic H2 Production by [Co(PtBu2NPh2)-(CH3CN)3](BF4)2. *Organometallics* **2010**, *29* (21), 5390−5401.
(19) Berben, L. A.; Peters, J. C. Hydrogen Evolution by Cobalt Tetraimine Catalysts Adsorbed on Electrode Surfaces. *Chem. Commun.* **2010**, *46* (3), 398−400.
(20) Szymczak, N. K.; Berben, L. A.; Peters, J. C. Redox Rich Dicobalt Macrocycles as Templates for Multi-Electron Transformations. *Chem. Commun.* **2009**, No. 44, 6729−6731.
(21) Artero, V.; Chavarot-Kerlidou, M.; Fontecave, M. Splitting Water with Cobalt. *Angew. Chem., Int. Ed.* **2011**, *50* (32), 7238−7266.
(22) McCrory, C. C. L.; Uyeda, C.; Peters, J. C. Electrocatalytic Hydrogen Evolution in Acidic Water with Molecular Cobalt Tetraazamacrocycles. *J. Am. Chem. Soc.* **2012**, *134* (6), 3164−3170.
(23) Chen, J.; Vannucci, A. K.; Mebi, C. A.; Okumura, N.; Borowski, S. C.; Swenson, M.; Lockett, L. T.; Evans, D. H.; Glass, R. S.; Lichtenberger, D. L. Synthesis of Diiron Hydrogenase Mimics Bearing Hydroquinone and Related Ligands. Electrochemical and Computational Studies of the Mechanism of Hydrogen Production and the Role of O−H···S Hydrogen Bonding. *Organometallics* **2010**, *29* (21), 5330−5340.
(24) Tard, C.; Pickett, C. J. Structural and Functional Analogues of the Active Sites of the [Fe]-, [NiFe]-, and [FeFe]-Hydrogenases. *Chem. Rev.* **2009**, *109* (6), 2245−2274.
(25) Chong, D.; Georgakaki, I. P.; Mejia-Rodriguez, R.; Sanabria-Chinchilla, J.; Soriaga, M. P.; Darensbourg, M. Y. Electrocatalysis of Hydrogen Production by Active Site Analogues of the Iron Hydrogenase Enzyme: Structure/Function Relationships. *Dalton Trans.* **2003**, No. 21, 4158−4163.
(26) Ott, S.; Kritikos, M.; Åkermark, B.; Sun, L.; Lomoth, R. A Biomimetic Pathway for Hydrogen Evolution from a Model of the Iron Hydrogenase Active Site. *Angew. Chem., Int. Ed.* **2004**, *43* (8), 1006−1009.
(27) Mejia-Rodriguez, R.; Chong, D.; Reibenspies, J. H.; Soriaga, M. P.; Darensbourg, M. Y. The Hydrophilic Phosphatriazaadamantane Ligand in the Development of H2 Production Electrocatalysts: Iron Hydrogenase Model Complexes. *J. Am. Chem. Soc.* **2004**, *126* (38), 12004−12014.
(28) Curtis, C. J.; Miedaner, A.; Ciancanelli, R.; Ellis, W. W.; Noll, B. C.; Rakowski DuBois, M.; DuBois, D. L. [Ni-(Et2PCH2NMeCH2PEt2)2]2+ as a Functional Model for Hydrogenases. *Inorg. Chem.* **2003**, *42* (1), 216−227.
(29) Collman, J. P.; Wagenknecht, P. S.; Hutchison, J. E.; Lewis, N. S.; Lopez, M. A.; Guilard, R.; L'Her, M.; Bothner-By, A. A.; Mishra, P. K. Dihydrogen Complexes of Metalloporphyrins: Characterization and Catalytic Hydrogen Oxidation Activity. *J. Am. Chem. Soc.* **1992**, *114* (14), 5654−5664.


https://doi.org/10.1021/acsorginorgau.4c00073
ACS Org. Inorg. Au 2025, 5, 105−116

(30) Ogo, S. Electrons from Hydrogen. *Chem. Commun.* **2009**, No. 23, 3317−3325.
(31) Kuwata, S.; Ikariya, T. Quest for Metal/NH Bifunctional Bioinspired Catalysis in a Dinuclear Platform. *Dalton Trans.* **2010**, *39* (12), 2984−2992.
(32) Yang, J. Y.; Bullock, R. M.; Shaw, W. J.; Twamley, B.; Fraze, K.; DuBois, M. R.; DuBois, D. L. Mechanistic Insights into Catalytic h(2) Oxidation by Ni Complexes Containing a Diphosphine Ligand with a Positioned Amine Base. *J. Am. Chem. Soc.* **2009**, *131* (16), 5935−5945.
(33) Camara, J. M.; Rauchfuss, T. B. Mild Redox Complementation Enables H2 Activation by [FeFe]-Hydrogenase Models. *J. Am. Chem. Soc.* **2011**, *133* (21), 8098−8101.
(34) Yang, J. Y.; Chen, S.; Dougherty, W. G.; Kassel, W. S.; Bullock, R. M.; DuBois, D. L.; Raugei, S.; Rousseau, R.; Dupuis, M.; DuBois, M. R. Hydrogen Oxidation Catalysis by a Nickel Diphosphine Complex with Pendant Tert-Butyl Amines. *Chem. Commun.* **2010**, *46* (45), 8618−8620.
(35) Camara, J. M.; Rauchfuss, T. B. Combining Acid-Base, Redox and Substrate Binding Functionalities to Give a Complete Model for the [FeFe]-Hydrogenase. *Nat. Chem.* **2012**, *4* (1), 26−30.
(36) Liu, T.; Dubois, D. L.; Bullock, R. M. An Iron Complex with Pendent Amines as a Molecular Electrocatalyst for Oxidation of Hydrogen. *Nat. Chem.* **2013**, *5* (3), 228−233.
(37) Gloaguen, F.; Rauchfuss, T. B. Small Molecule Mimics of Hydrogenases: Hydrides and Redox. *Chem. Soc. Rev.* **2009**, *38* (1), 100−108.
(38) Ringenberg, M. R.; Nilges, M. J.; Rauchfuss, T. B.; Wilson, S. R. Oxidation of Dihydrogen by Iridium Complexes of Redox-Active Ligands. *Organometallics* **2010**, *29* (8), 1956−1965.
(39) Ringenberg, M. R.; Kokatam, S. L.; Heiden, Z. M.; Rauchfuss, T. B. Redox-Switched Oxidation of Dihydrogen Using a Non-Innocent Ligand. *J. Am. Chem. Soc.* **2008**, *130* (3), 788−789.
(40) Vignais, P. M.; Billoud, B. Occurrence, Classification, and Biological Function of Hydrogenases: An Overview. *Chem. Rev.* **2007**, *107* (10), 4206−4272.
(41) Vincent, K. A.; Parkin, A.; Armstrong, F. A. Investigating and Exploiting the Electrocatalytic Properties of Hydrogenases. *Chem. Rev.* **2007**, *107* (10), 4366−4413.
(42) Lubitz, W.; Ogata, H.; Rüdiger, O.; Reijerse, E. Hydrogenases. *Chem. Rev.* **2014**, *114* (8), 4081−4148.
(43) Amanullah, S.; Saha, P.; Nayek, A.; Ahmed, M. E.; Dey, A. Biochemical and Artificial Pathways for the Reduction of Carbon Dioxide, Nitrite and the Competing Proton Reduction: Effect of 2ndsphere Interactions in Catalysis. *Chem. Soc. Rev.* **2021**, *50* (6), 3755−3823.
(44) Nayek, A.; Ahmed, M. E.; Samanta, S.; Dinda, S.; Patra, S.; Dey, S. G.; Dey, A. Bioinorganic Chemistry on Electrodes: Methods to Functional Modeling. *J. Am. Chem. Soc.* **2022**, *144* (19), 8402−8429.
(45) Volbeda, A.; Charon, M.-H.; Piras, C.; Hatchikian, E. C.; Frey, M.; Fontecilla-Camps, J. C. Crystal Structure of the Nickel−Iron Hydrogenase from Desulfovibrio Gigas. *Nature* **1995**, *373* (6515), 580−587.
(46) Wittkamp, F.; Senger, M.; Stripp, S. T.; Apfel, U.-P. [FeFe]-Hydrogenases: Recent Developments and Future Perspectives. *Chem. Commun.* **2018**, *54* (47), 5934−5942.
(47) Esselborn, J.; Muraki, N.; Klein, K.; Engelbrecht, V.; Metzler-Nolte, N.; Apfel, U.-P.; Hofmann, E.; Kurisu, G.; Happe, T. A Structural View of Synthetic Cofactor Integration into [FeFe]-Hydrogenases. *Chem. Sci.* **2016**, *7* (2), 959−968.
(48) Nicolet, Y.; Piras, C.; Legrand, P.; Hatchikian, C. E.; Fontecilla-Camps, J. C. Desulfovibrio Desulfuricans Iron Hydrogenase: The Structure Shows Unusual Coordination to an Active Site Fe Binuclear Center. *Structure* **1999**, *7* (1), 13−23.
(49) Peters, J. W.; Lanzilotta, W. N.; Lemon, B. J.; Seefeldt, L. C. X-ray Crystal Structure of the Fe-Only Hydrogenase (CpI) from Clostridium pasteurianum to 1.8 Angstrom Resolution. *Science* **1998**, *282* (5395), 1853−1858.
(50) Roseboom, W.; De Lacey, A. L.; Fernandez, V. M.; Hatchikian, E. C.; Albracht, S. P. J. The Active Site of the [FeFe]-Hydrogenase from Desulfovibrio Desulfuricans. II. Redox Properties, Light Sensitivity and CO-Ligand Exchange as Observed by Infrared Spectroscopy. *J. Biol. Inorg. Chem.* **2006**, *11* (1), 102−118.
(51) Chen, Z.; Lemon, B. J.; Huang, S.; Swartz, D. J.; Peters, J. W.; Bagley, K. A. Infrared Studies of the CO-Inhibited Form of the Fe-Only Hydrogenase from Clostridium Pasteurianum I: Examination of Its Light Sensitivity at Cryogenic Temperatures. *Biochemistry* **2002**, *41* (6), 2036−2043.
(52) Darensbourg, M. Y.; Lyon, E. J.; Zhao, X.; Georgakaki, I. P. The Organometallic Active Site of [Fe]Hydrogenase: Models and Entatic States. *Proc. Natl. Acad. Sci. U. S. A.* **2003**, *100* (7), 3683−3688.
(53) Nicolet, Y.; de Lacey, A. L.; Vernède, X.; Fernandez, V. M.; Hatchikian, E. C.; Fontecilla-Camps, J. C. Crystallographic and FTIR Spectroscopic Evidence of Changes in Fe Coordination Upon Reduction of the Active Site of the Fe-Only Hydrogenase from Desulfovibrio Desulfuricans. *J. Am. Chem. Soc.* **2001**, *123* (8), 1596−1601.
(54) Nayek, A.; Dey, S.; Patra, S.; Rana, A.; Serrano, P. N.; George, S. J.; Cramer, S. P.; Ghosh Dey, S.; Dey, A. Facile Electrocatalytic Proton Reduction by a [Fe−Fe]-Hydrogenase Bio-Inspired Synthetic Model Bearing a Terminal CN− Ligand. *Chem. Sci.* **2024**, *15* (6), 2167−2180.
(55) Erdem, O. F.; Schwartz, L.; Stein, M.; Silakov, A.; Kaur-Ghumaan, S.; Huang, P.; Ott, S.; Reijerse, E. J.; Lubitz, W. A Model of the [FeFe] Hydrogenase Active Site with a Biologically Relevant Azadithiolate Bridge: A Spectroscopic and Theoretical Investigation. *Angew. Chem., Int. Ed.* **2011**, *50* (6), 1439−1443.
(56) Lubitz, W.; Reijerse, E.; van Gastel, M. [NiFe] and [FeFe] Hydrogenases Studied by Advanced Magnetic Resonance Techniques. *Chem. Rev.* **2007**, *107* (10), 4331−4365.
(57) Silakov, A.; Wenk, B.; Reijerse, E.; Lubitz, W. 14N HYSCORE Investigation of the H-Cluster of [FeFe] Hydrogenase: Evidence for a Nitrogen in the Dithiol Bridge. *Phys. Chem. Chem. Phys.* **2009**, *11* (31), 6592−6599.
(58) Sommer, C.; Adamska-Venkatesh, A.; Pawlak, K.; Birrell, J. A.; Rüdiger, O.; Reijerse, E. J.; Lubitz, W. Proton Coupled Electronic Rearrangement within the H-Cluster as an Essential Step in the Catalytic Cycle of [FeFe] Hydrogenases. *J. Am. Chem. Soc.* **2017**, *139* (4), 1440−1443.
(59) Birrell, J. A.; Pelmenschikov, V.; Mishra, N.; Wang, H.; Yoda, Y.; Tamasaku, K.; Rauchfuss, T. B.; Cramer, S. P.; Lubitz, W.; DeBeer, S. Spectroscopic and Computational Evidence That [FeFe] Hydrogenases Operate Exclusively with CO-Bridged Intermediates. *J. Am. Chem. Soc.* **2020**, *142* (1), 222−232.
(60) Mulder, D. W.; Guo, Y.; Ratzloff, M. W.; King, P. W. Identification of a Catalytic Iron-Hydride at the H-Cluster of [FeFe]-Hydrogenase. *J. Am. Chem. Soc.* **2017**, *139* (1), 83−86.
(61) Ratzloff, M. W.; Artz, J. H.; Mulder, D. W.; Collins, R. T.; Furtak, T. E.; King, P. W. CO-Bridged H-Cluster Intermediates in the Catalytic Mechanism of [FeFe]-Hydrogenase CaI. *J. Am. Chem. Soc.* **2018**, *140* (24), 7623−7628.
(62) Sanchez, M. L. K.; Sommer, C.; Reijerse, E.; Birrell, J. A.; Lubitz, W.; Dyer, R. B. Investigating the Kinetic Competency of CrHydA1 [FeFe] Hydrogenase Intermediate States via Time-Resolved Infrared Spectroscopy. *J. Am. Chem. Soc.* **2019**, *141* (40), 16064−16070.
(63) Senger, M.; Mebs, S.; Duan, J.; Shulenina, O.; Laun, K.; Kertess, L.; Wittkamp, F.; Apfel, U.-P.; Happe, T.; Winkler, M.; Haumann, M.; Stripp, S. T. Protonation/Reduction Dynamics at the [4Fe−4S] Cluster of the Hydrogen-Forming Cofactor in [FeFe]-Hydrogenases. *Phys. Chem. Chem. Phys.* **2018**, *20* (5), 3128−3140.
(64) Berggren, G.; Adamska, A.; Lambertz, C.; Simmons, T. R.; Esselborn, J.; Atta, M.; Gambarelli, S.; Mouesca, J. M.; Reijerse, E.; Lubitz, W.; Happe, T.; Artero, V.; Fontecave, M. Biomimetic Assembly and Activation of [FeFe]-Hydrogenases. *Nature* **2013**, *499* (7456), 66−69.


https://doi.org/10.1021/acsorginorgau.4c00073
*ACS Org. Inorg. Au* 2025, 5, 105−116

(65) Land, H.; Senger, M.; Berggren, G.; Stripp, S. T. Current State of [FeFe]-Hydrogenase Research: Biodiversity and Spectroscopic Investigations. *ACS Catal.* **2020**, *10* (13), 7069−7086.
(66) Kisgeropoulos, E. C.; Artz, J. H.; Blahut, M.; Peters, J. W.; King, P. W.; Mulder, D. W. Properties of the Iron-Sulfur Cluster Electron Transfer Relay in an [FeFe]-Hydrogenase That Is Tuned for H2 Oxidation Catalysis. *J. Biol. Chem.* **2024**, *300*, 107292.
(67) Olsen, M. T.; Barton, B. E.; Rauchfuss, T. B. Hydrogen Activation by Biomimetic Diiron Dithiolates. *Inorg. Chem.* **2009**, *48* (16), 7507−7509.
(68) Camara, J. M.; Rauchfuss, T. B. Combining Acid−Base, Redox and Substrate Binding Functionalities to Give a Complete Model for the [FeFe]-Hydrogenase. *Nat. Chem.* **2012**, *4* (1), 26−30.
(69) Wang, N.; Wang, M.; Wang, Y.; Zheng, D.; Han, H.; Ahlquist, M. S. G.; Sun, L. Catalytic Activation of H2 under Mild Conditions by an [FeFe]-Hydrogenase Model via an Active $\mu$-Hydride Species. *J. Am. Chem. Soc.* **2013**, *135* (37), 13688−13691.
(70) Cheng, M.; Wang, M.; Zheng, D.; Sun, L. Effect of the S-to-S Bridge on the Redox Properties and H2 Activation Performance of Diiron Complexes Related to the [FeFe]-Hydrogenase Active Site. *Dalton Trans.* **2016**, *45* (44), 17687−17696.
(71) Dutta, A.; Appel, A. M.; Shaw, W. J. Designing Electrochemically Reversible H2 Oxidation and Production Catalysts. *Nat. Rev. Chem.* **2018**, *2* (9), 244−252.
(72) DuBois, D. L. Development of Molecular Electrocatalysts for Energy Storage. *Inorg. Chem.* **2014**, *53* (8), 3935−3960.
(73) Wiedner, E. S.; Appel, A. M.; Raugei, S.; Shaw, W. J.; Bullock, R. M. Molecular Catalysts with Diphosphine Ligands Containing Pendant Amines. *Chem. Rev.* **2022**, *122* (14), 12427−12474.
(74) Bullock, R. M.; Helm, M. L. Molecular Electrocatalysts for Oxidation of Hydrogen Using Earth-Abundant Metals: Shoving Protons Around with Proton Relays. *Acc. Chem. Res.* **2015**, *48* (7), 2017−2026.
(75) DuBois, D. L.; Bullock, R. M. Molecular Electrocatalysts for the Oxidation of Hydrogen and the Production of Hydrogen − The Role of Pendant Amines as Proton Relays. *Eur. J. Inorg. Chem.* **2011**, *2011* (7), 1017−1027.
(76) Yang, J. Y.; Smith, S. E.; Liu, T.; Dougherty, W. G.; Hoffert, W. A.; Kassel, W. S.; DuBois, M. R.; DuBois, D. L.; Bullock, R. M. Two Pathways for Electrocatalytic Oxidation of Hydrogen by a Nickel Bis(Diphosphine) Complex with Pendant Amines in the Second Coordination Sphere. *J. Am. Chem. Soc.* **2013**, *135* (26), 9700−9712.
(77) Liu, T.; DuBois, M. R.; DuBois, D. L.; Bullock, R. M. Electrochemical Oxidation of H2 Catalyzed by Ruthenium Hydride Complexes Bearing P2N2 Ligands with Pendant Amines as Proton Relays. *Energy Environ. Sci.* **2014**, *7* (11), 3630−3639.
(78) Ahmed, M. E.; Dey, S.; Darensbourg, M. Y.; Dey, A. Oxygen-Tolerant H2 Production by [FeFe]-H2ase Active Site Mimics Aided by Second Sphere Proton Shuttle. *J. Am. Chem. Soc.* **2018**, *140* (39), 12457−12468.
(79) Ahmed, M. E.; Nayek, A.; Križan, A.; Coutard, N.; Morozan, A.; Ghosh Dey, S.; Lomoth, R.; Hammarström, L.; Artero, V.; Dey, A. A Bidirectional Bioinspired [FeFe]-Hydrogenase Model. *J. Am. Chem. Soc.* **2022**, *144* (8), 3614−3625.
(80) Ahmed, M. E.; Dey, S.; Mondal, B.; Dey, A. H2 Evolution Catalyzed by a FeFe-Hydrogenase Synthetic Model Covalently Attached to Graphite Surfaces. *Chem. Commun.* **2017**, *53* (58), 8188−8191.
(81) Dey, S.; Rana, A.; Dey, S. G.; Dey, A. Electrochemical Hydrogen Production in Acidic Water by an Azadithiolate Bridged Synthetic Hydrogenese Mimic: Role of Aqueous Solvation in Lowering Overpotential. *ACS Catal.* **2013**, *3* (3), 429−436.
(82) Dey, A.; Ahmed, M. E.; Das, P.; Ahamed, S. M.; Chattopadhyay, S.; Nayek, A.; Mondal, M.; Malik, S. Amplifying Reactivity of Bio-Inspired [FeFe]-Hydrogenase Mimics by Organic Nanotubes. *Chem. - Eur. J.* **2024**, No. e202403011.
(83) Ott, S.; Borgström, M.; Kritikos, M.; Lomoth, R.; Bergquist, J.; Åkermark, B.; Hammarström, L.; Sun, L. Model of the Iron Hydrogenase Active Site Covalently Linked to a Ruthenium Photosensitizer: Synthesis and Photophysical Properties. *Inorg. Chem.* **2004**, *43* (15), 4683−4692.
(84) Liu, T.; Wang, M.; Shi, Z.; Cui, H.; Dong, W.; Chen, J.; Åkermark, B.; Sun, L. Synthesis, Structures and Electrochemical Properties of Nitro- and Amino-Functionalized Diiron Azadithiolates as Active Site Models of Fe-Only Hydrogenases. *Chem. − A Eur. J* **2004**, *10* (18), 4474−4479.
(85) Jiang, S.; Liu, J.; Shi, Y.; Wang, Z.; Åkermark, B.; Sun, L. Fe−S Complexes Containing Five-Membered Heterocycles: Novel Models for the Active Site of Hydrogenases with Unusual Low Reduction Potential. *Dalton Trans.* **2007**, No. 8, 896−902.
(86) Harb, M. K.; Apfel, U.-P.; Kübel, J.; Görls, H.; Felton, G. A. N.; Sakamoto, T.; Evans, D. H.; Glass, R. S.; Lichtenberger, D. L.; El-Khateeb, M.; Weigand, W. Preparation and Characterization of Homologous Diiron Dithiolato, Diselenato, and Ditellurato Complexes: [FeFe]-Hydrogenase Models. *Organometallics* **2009**, *28* (23), 6666−6675.
(87) Jiang, S.; Liu, J.; Shi, Y.; Wang, Z.; Åkermark, B.; Sun, L. Preparation, characteristics and crystal structures of novel N-heterocyclic carbene substituted furan- and pyridine-containing azadithiolate Fe−S complexes. *Polyhedron* **2007**, *26* (7), 1499−1504.
(88) Kaljurand, I.; Kütt, A.; Sooväli, L.; Rodima, T.; Mäemets, V.; Leito, I.; Koppel, I. A. Extension of the Self-Consistent Spectrophotometric Basicity Scale in Acetonitrile to a Full Span of 28 PKa Units: Unification of Different Basicity Scales. *J. Org. Chem.* **2005**, *70* (3), 1019−1028.
(89) Nicholson, R. S.; Shain, I. Theory of Stationary Electrode Polarography. Single Scan and Cyclic Methods Applied to Reversible, Irreversible, and Kinetic Systems. *Anal. Chem.* **1964**, *36* (4), 706−723.
(90) Bard, A. J.; Faulkner, L. R. *Electrochemical Methods: Fundamentals and Applications*, 2nd ed.; John Wiley & Sons: New York, 2001.
(91) Liu, T.; Liao, Q.; O'Hagan, M.; Hulley, E. B.; DuBois, D. L.; Bullock, R. M. Iron Complexes Bearing Diphosphine Ligands with Positioned Pendant Amines as Electrocatalysts for the Oxidation of H2. *Organometallics* **2015**, *34* (12), 2747−2764.
(92) Darmon, J. M.; Raugei, S.; Liu, T.; Hulley, E. B.; Weiss, C. J.; Bullock, R. M.; Helm, M. L. Iron Complexes for the Electrocatalytic Oxidation of Hydrogen: Tuning Primary and Secondary Coordination Spheres. *ACS Catal.* **2014**, *4* (4), 1246−1260.
(93) Roy, S.; Sharma, B.; Pécaut, J.; Simon, P.; Fontecave, M.; Tran, P. D.; Derat, E.; Artero, V. Molecular Cobalt Complexes with Pendant Amines for Selective Electrocatalytic Reduction of Carbon Dioxide to Formic Acid. *J. Am. Chem. Soc.* **2017**, *139* (10), 3685−3696.
(94) Savéant, J. M.; Vianello, E. Potential-Sweep Voltammetry: General Theory of Chemical Polarization. *Electrochim. Acta* **1967**, *12* (6), 629−646.
(95) Saveant, J. M.; Vianello, E. Potential-Sweep Chronoamperometry: Kinetic Currents for First-Order Chemical Reaction Parallel to Electron-Transfer Process (Catalytic Currents). *Electrochim. Acta* **1965**, *10* (9), 905−920.
(96) Fourmond, V.; Jacques, P.-A.; Fontecave, M.; Artero, V. H2 Evolution and Molecular Electrocatalysts: Determination of Overpotentials and Effect of Homoconjugation. *Inorg. Chem.* **2010**, *49* (22), 10338−10347.
(97) Smith, S. E.; Yang, J. Y.; DuBois, D. L.; Bullock, R. M. Reversible Electrocatalytic Production and Oxidation of Hydrogen at Low Overpotentials by a Functional Hydrogenase Mimic. *Angew. Chem., Int. Ed.* **2012**, *51* (13), 3152−3155.
(98) Wang, S.; Pullen, S.; Weippert, V.; Liu, T.; Ott, S.; Lomoth, R.; Hammarström, L. Direct Spectroscopic Detection of Key Intermediates and the Turnover Process in Catalytic H2 Formation by a Biomimetic Diiron Catalyst. *Chem. - Eur. J.* **2019**, *25* (47), 11135−11140.
(99) Borg, S. J.; Tye, J. W.; Hall, M. B.; Best, S. P. Assignment of Molecular Structures to the Electrochemical Reduction Products of Diiron Compounds Related to [Fe−Fe] Hydrogenase: A Combined Experimental and Density Functional Theory Study. *Inorg. Chem.* **2007**, *46* (2), 384−394.

(100) Olsen, M. T.; Rauchfuss, T. B.; Wilson, S. R. Role of the Azadithiolate Cofactor in Models for [FeFe]-Hydrogenase: Novel Structures and Catalytic Implications. *J. Am. Chem. Soc.* **2010**, *132* (50), 17733−17740.
(101) Spek, A. L. Single-Crystal Structure Validation with the Program {\it PLATON}. *J. Appl. Crystallogr.* **2003**, *36* (1), 7−13.
(102) Spek, A. L. Structure Validation in Chemical Crystallography. *Acta Crystallogr., Sect. D* **2009**, *65* (2), 148−155.
(103) Sheldrick, G. M. Crystal structure refinement with SHELXL. *Acta Crystallogr., Sect. C: Struct. Chem.* **2015**, *71* (1), 3−8.
(104) Dolomanov, O. V.; Bourhis, L. J.; Gildea, R. J.; Howard, J. A. K.; Puschmann, H. {\it OLEX2}: A Complete Structure Solution, Refinement and Analysis Program. *J. Appl. Crystallogr.* **2009**, *42* (2), 339−341.
(105) Frisch, M. J.; Trucks, G. W.; Schlegel, H. B.; Scuseria, G. E.; Robb, M. A.; Cheeseman, J. R.; Scalmani, G.; Barone, V.; Petersson, G. A.; Nakatsuji, H., et al. *G16_C01 Gaussian 16, Revision C.01*, Gaussian, Inc., 2016.
(106) Perdew, J. P. Density-Functional Approximation for the Correlation Energy of the Inhomogeneous Electron Gas. *Phys. Rev. B* **1986**, *33* (12), 8822−8824.
(107) Becke, A. D. Density-Functional Exchange-Energy Approximation with Correct Asymptotic Behavior. *Phys. Rev. A* **1988**, *38* (6), 3098−3100.


https://doi.org/10.1021/acsorginorgau.4c00073
*ACS Org. Inorg. Au* 2025, 5, 105−116